Spatially-Resolved Elemental Analysis
in the Scanning Electron Microscope

Report for the Advanced Lab Course

by

Yoshua Hempel

and

William Wenig

supervised by Dr. Alberto Eljarrat

July 2022, Berlin

Humboldt-Universität zu Berlin
Institut für Physik

Contents

Abstract

In this experiment we acquainted ourselves with the functionality of a scanning electron microscope and its utility for generating high resolution gray scale images and elemental maps, as well as X-ray spectroscopy. We used the SLM's Everhart Thornley and inlens detectors at acceleration voltages of 5 keV and 15 keV to image a Silicone substrate and the Silicone-Germanium crystals which were grown on it and compared the results. Using these images we calculated the height of the Si-Ge crystals to be $h = 51(8)$ nm. With the SLM's EDS detector we analyzed the X-ray spectra of the substrate and the crystals and created elemental maps.

Introduction

The way of modern electron microscopy was paved by Manfred von Ardenne 85 years ago, with the invention of the first scanning electron microscope that was able to produce high resolution images of studied specimen. In this lab, instead of looking back and analyzing how it all began, we will rather explore the basic scope and working principle of a modern scanning electron microscope and its detectors. To do so, we utilized the high-end »ZEISS GeminiSEM 500«, with a maximum resolution of 0.6 nm at 15 kV acceleration voltage [Car]. We will use it to analyze a sample of nanostructures (see [Zhe+12]) consisting of single-crystalline (Si,Ge) islands grown on an Si substrate. Each island satisfies the geometry of a frustum of a pyramid with square base. Analyzing the sample, we will acquire high-quality gray scale images of the islands from both the Inlens and Everhart-Thornley detector, obtain X-ray spectra produced by the incident beam and spatially map the composition of the sample[1]. All tasks were carried out at 5 kV and 15 kV acceleration voltage and yielded results for the mean height and the chemical composition of the islands.

1. Comparison of gray scale images

At first we will compare the gray scale images we obtained by using the Inlens and Everhart-Thornley detector. The images are illustrated in Figure 1 and were achieved after we underwent the instructed steps in [Par+16] with additional advice from our supervisor Dr. Eljarrat. The first comparisons we are going over will involve the influence of the beam energy on the resulting image.

1.1. Beam energy influence on Inlens detector

Looking at the acquired images with the Inlens detector we notice a decrease in noise and deterioration in resolution when lowering the acceleration voltage from 15 kV in Figure 1d to 5kV in 1c. We only note the reduction of noise here and discuss it in section 1.3. The observed behavior

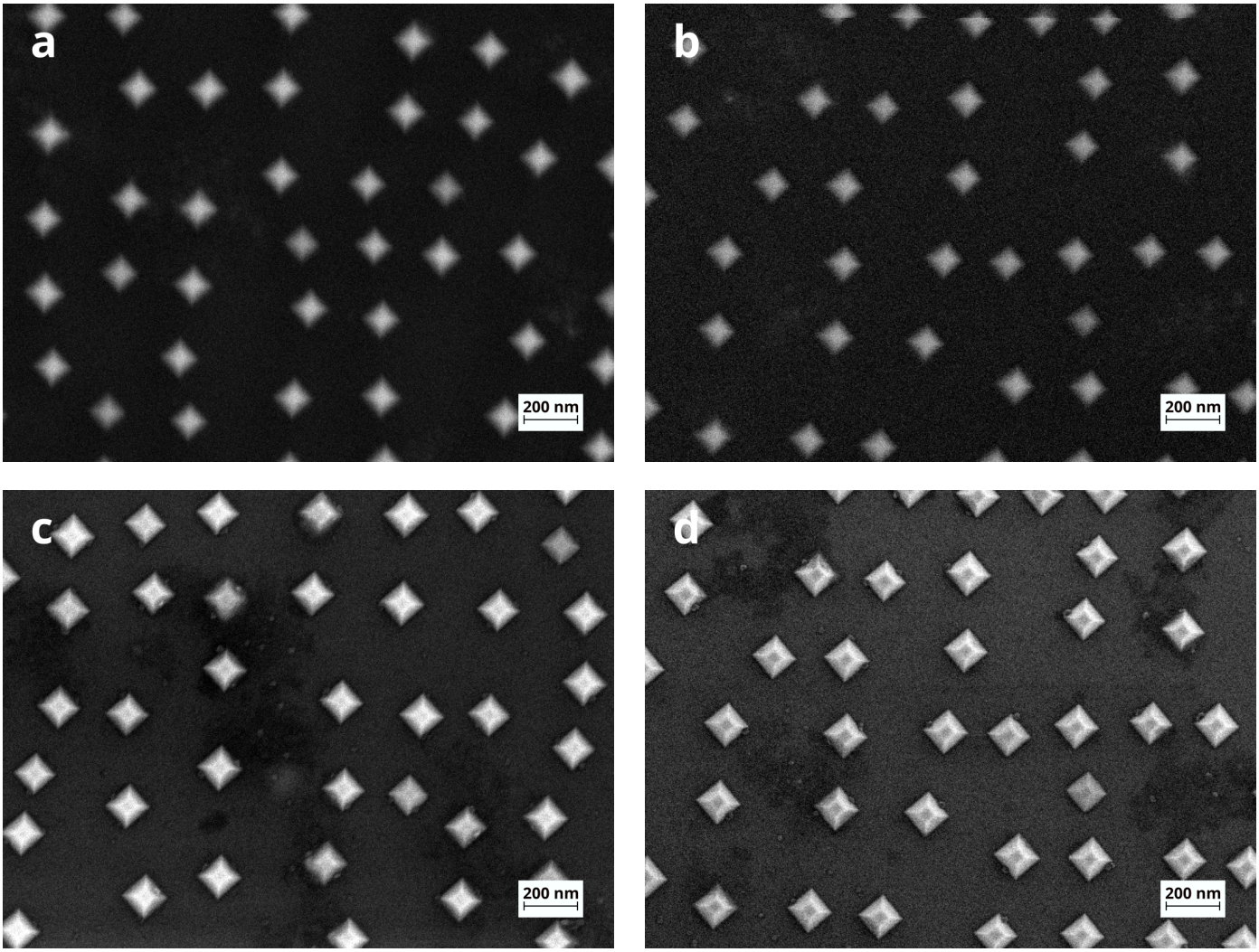

Figure 1: Acquired gray scale images from the Inlens and ET detector at 50k magnification and aperture of 20 µm with different acceleration voltages: (a) ET at 5 kV, (b) ET at 15 kV, (c) Inlens at 5 kV and (d) ET at 15 kV.

[1]Therefor we use a Bruker Quantax EDS system with a 30 mm^2 Xflash 6-30 silicon drift detector.

of the resolution can be explained by considering which kinds of secondary electrons (SE) the Inlens detector is effectively measuring and how their emerging position changes with different beam energies. As stated in [Par+16] (see Section »2.3.2 Detectors«) and [Gol+18] (see Section »14.3.3 "Through-the-Lens" Detectors«)[1], the Inlens detector is very efficient in collecting SE that emerge close to the beam because of the small action radius of the electrostatic lense the GeminiSEM 500 is using. If we are using the maximum beam energy of the SEM, the interaction volume (Figure 2.4 of [Par+16]) will have maximum lateral spread. Because the collected SE1 are still generated at the position the beam impinges the sample, the spread of the interaction volume will diminish the contribution of the SE2. When the ratio of collected SE1 to SE2 increases the resolution will also increase because SE1 retain high resolution information at the scale of the beam entrance footprint. Thereby higher beam energies will result in higher resolution images for the Inlens detector with the caveat of noise mentioned in section 1.3.

1.2. Beam energy influence on ET detector

Going on with the images at different beam energies for the ET detector we notice a decrease in noise and an improvement in resolution from 15 kV in Figure 1b to 5 kV in 1a. This observed improvement is smaller than the deterioration of resolution in the previous section. The ET detector detects all kinds of SE as well as BSE (see [Par+16] Section 2.3 and [Gol+18] Section 14.3.1). Which makes this detector subject to the degraded spatial resolution of the SE2, SE3 and BSE at a higher beam energies. As mentioned in the previous section the increase in the interaction volume for higher beam energies will cause the SE2, SE3 and BSE to emerge at distances outside of the dimensions of the focused beam footprint and thus degrading the spatial resolution of these measured electrons. On the other hand if we lower the beam energy as suggested in [Gol+18] section 14.4.4 »High Resolution SEM Imaging« the collected electrons by the ET detector will contain more spatial information. This means that for the ET detector a lower beam energy yields better image resolution.

1.3. Noise performance

Clearly visible all images shown in Figure 1 contain a certain amount of noise. We observed in section 1.1 and 1.2 that with lower beam energy the noise decreases. This can again be explained via the dimension of the interaction volume. Because the SE1 are generated on the position of beam impingement, they contribute the most amount of local topological information. The SE2, SE3 and BSE on the other hand "average" out the topological information over a bigger area on the scale of µm and create noise that is dependent on the interaction volume. Because the ET detector is more sensitive towards these electrons, the decrease in noise is very noticeable when going from Figure 1b to Figure 1a.

[1] It should be mentioned that in this resource the authors are talking about an SEM with magnetic immersion lenses also mentioned in Section 2.3.1 of [Par+16]. The GeminiSEM 500 uses an electrostatic lens that collects SE1 and SE2 close to the primary beam as well.

1.4. Detector efficiencies compared

Comparing the images acquired through the Inlens detector in 1a and 1b with the ones acquired by the ET detector in 1c and 1d the difference in resolution stands out. The Inlense detector yields a far better image for the analysis of topological information on this scale hence we are going to use it in the following sections for the height determination of the islands. The Inlens detector achieves this better resolution because it collects a bigger fraction of SE1 than SE2 whereas the ET detector is collecting a bigger fraction of all other kinds of SE2,SE3 and BSE than SE1. The Inlens detector therefore "filters" out the signal degradation that is inherent to the SE that are not SE1.

2. Height determination

In this section we'll present how we used the images we acquired with the SEM, to approximate the height of the frustums. For this we worked with images acquired with the inlens detector at a 15 kV voltage, as that resulted in the best images. The height can be calculated by measuring the horizontal distance l of the edges of the island to the top facet and assuming an inclination angle of $\theta = 55°$. With this the height can be calculated using the following formula.

$$h = l \cdot \tan\theta \tag{2.1}$$

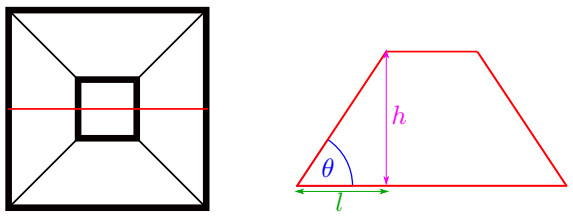

(a) Position of the crosssection (b) Crossection of the frustum

Figure 2: Depiction of the assumed geometry and measured distances

In order to measure the distance l, we first had to rotate the images[1] such that the edges of the islands were as parallel to the respective horizontal and vertical axes of the image as possible. This was done for the entire image as a whole, so every island was rotated by the same angle ϕ, which was approximately 50.6°. Ideally this process would have been repeated for each island individually, as there could be some variance in the islands' orientation. We then manually cut out, what we perceived to be the top facet of the frustums, such that the alpha channel of the image has a value of 0 at the places of the top facets and 255 everywhere else. For ap-

[1] the initial image processing was done using Gimp 2.10.14

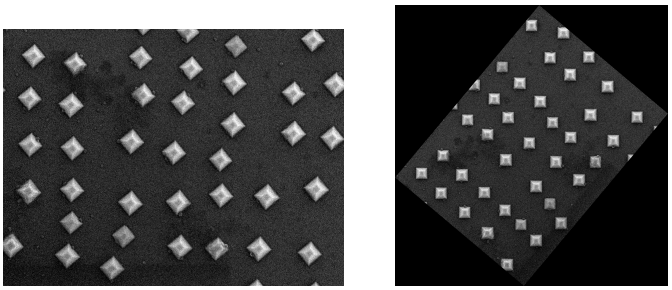

Figure 3: SEM image before (left) and after (right) rotation

proximating the position of the top facet, we used the fact that the brightness of the image should ideally have a local maximum at convex edges, as explained in [Gol+18] page 151 onwards. This happens because the surface area immediately around the incident beam is maximized, increasing the volume of SE_1 electrons. After this, every island was cut out and saved as a separate image.

Figure 4: Example of a cut-out frustum

Now we used the alpha channel of these images to measure l, by counting the pixels between the middle of each edge of the image and the top facet. This was done by extracting the alpha channel of the image as an array using the Python library `imageio`, followed by applying a filter in the form of another array, which has half a row or column of ones in between the center of the image and the edge from which we want to measure l and zeros everywhere else. Calculating the sum of the resulting array and dividing by 255 returns the amount of pixels between the edge of the image and the rectangle representing the top facet. To get l we then had to multiply the amount of pixels with the pixel-size, which for each image is 1 px = 2.215 nm[2]. With the chosen model of the frustums as one rectangle inside another, these four lengths completely describe the geometry of the images. This process was applied to a total of 80 islands extracted from three separate images. Since it is possible that the substrate wasn't exactly at a right angle to the electron beam, there could have been a systematic error in the length l, depending on the edge from which the distance was measured. Because of this we first calculated the mean and standard deviation[3] of the heights for each side separately.

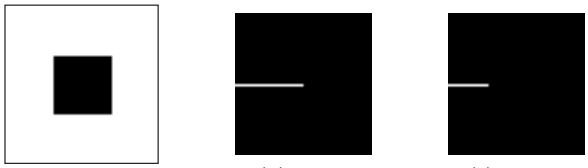

(a) Alpha channel of frustum (b) Filter (c) Result

Figure 5: Example of measurement process for the left side

Table 1: Arithmetic Mean and standard deviation of Calculated height h for different sides

	left	bottom	right	top
Mean of h [nm]	51	51	49	53
Standard deviation σ_h [nm]	4	4	5	4

The mean of all sides combined turned out to be $\overline{h} = 51$ nm, with a standard deviation of $\sigma_{\overline{h}} = 4$ nm. To get an approximation of the systematic error caused by misalignment of the sample, we used the maximal difference between the mean heights $u_{h,s} = 4$ nm. This was done since a deviation in the angle of the substrate to the electron beam could cause such differences. Since there is an absolute upper bound for how precise our measurements could be, given by the pixel size, we also include $u_{h,\mathrm{px}} = 1\ \mathrm{px} \tan 55° \approx 3$ nm in the total systematic uncertainty. We calculated the total uncertainty in the following way:

$$u_h = \sqrt{\sigma_{\overline{h}}^2 + (u_{h,\mathrm{px}} + u_{h,s})^2} = 8 \text{ nm} \tag{2.2}$$

So the final result of the height determination is as follows.

$$\boxed{h = 51(8) \text{ nm}} \tag{2.3}$$

3. Spectral analysis

For the analysis of the chemical composition of the (Si,Ge) islands, we had a dedicated Energy-dispersive X-ray spectroscopy (EDS) detector at our disposal that is built into the GeminiSEM 500. We utilized this Bruker Quantax system with an XFlash 6-30 detector to acquire spectra of the Si substrate and of the islands themselves at 5 kV and 15 kV acceleration voltage. We will start by looking at the gathered spectra for the acceleration voltage of 5 kV.

3.1. Spectra for 5 kV acceleration voltage

From the spectra shown in Figure 6, distinguishable peaks are visible. We found that when performing EDS the count peaks around energies close to zero are »strobe peaks« that arise from electronic noise from inside the silicon drift detector [WW03]. This strobe peak can be regarded as the spread function of the detector hence we are going to exclude it from Figure 6 to improve visibility of the nontrivial peaks we actually want to look at.

Figure 7 now highlights these nontrivial peaks of characteristic X-ray energies that the detector counted. It shows the spectra of the measurements we conducted on the Si substrate and on one of the (Si,Ge) islands for 5 kV. Looking at

[2] As specified in the images generated by the SLM

[3] with a divisor of $N - 1$

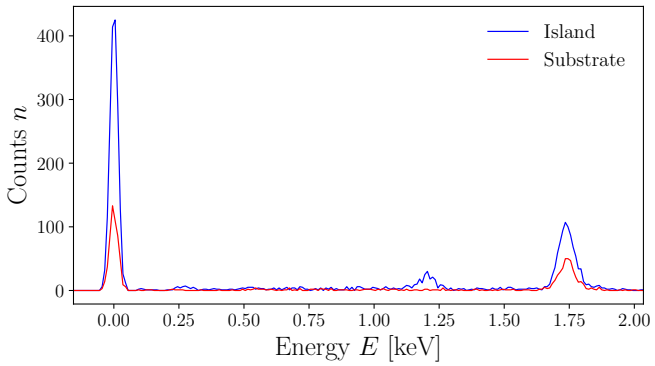

Figure 6: X-ray energies E counted by the XFlash detector on the position of an island and on the substrate itself with acceleration voltage 5 kV.

the spectrum we obtained from the substrate itself, we see a distinct peak at $E_{\mathrm{Si}} = 1.74$ keV. This peak corresponds to the Lα_1 transition depicted in Table 2 and 3 of Silicon.

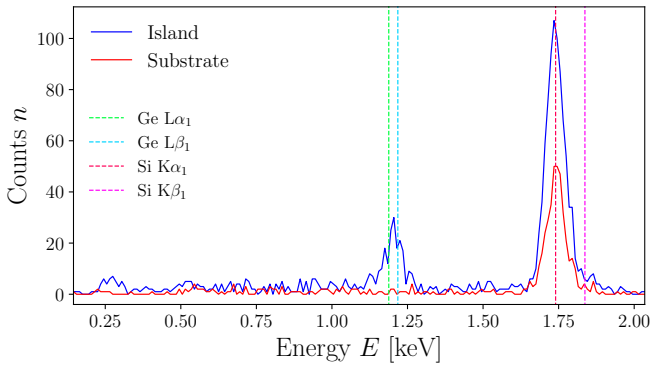

Figure 7: Spectra from Figure 6 without strobe peaks. Characteristic X-ray transitions displayed.

Table 2: X-ray transitions relevant for this analysis.

Transition	X-ray notation	Atomic notation
Lα_1	$M_5 \to L_3$	$3D_{5/2} \to 2P_{3/2}$
Lβ_1	$M_4 \to L_2$	$3D_{3/2} \to 2P_{1/2}$
Kα_1	$L_3 \to K$	$2P_{3/2} \to 1S_{1/2}$
Kβ_1	$M_3 \to K$	$3P_{3/2} \to 1S_{1/2}$

Although the usual resolution achieved in EDS is in the dimensions of 100 eV [WW03], it is visible that energies corresponding to the Lβ_1 transition of Si where not counted as much as the ones corresponding to Lα_1. Attempting to explain this phenomenon we found that for elements with $18 \leq Z \leq 39$ (see [SE72] Table I) and for elements with $Z = 47, 49, 52, 55$ and 56 (see [Mar+99] Table 2) the relative transition probability

$$\frac{P(\mathrm{K}\beta_1)}{P(\mathrm{K}\alpha_1)} \lessapprox \frac{1}{3}. \tag{3.1}$$

We suspect that Silicon with $Z = 14$ is going to follow this behavior, which explains why energies corresponding to the Kβ_1 transition are counted in such little amounts.

Table 3: Values for the X-ray energies corresponding to the transitions of Si and Ge for Table 2 from [Bru].

Element	Transition	Energy E [keV]
Si	Kα_1	1.740
Si	Kβ_1	1.837
Ge	Kα_1	9.886
Ge	Kβ_1	10.982
Ge	Lα_1	1.188
Ge	Lβ_1	1.218

As we just mentioned the resolution for EDS, it is certain that we won't be able to distinguish the count peaks for the transitions Lα_1 and Lβ_1 due to smaller energy difference

$$E(\mathrm{Ge}_{\mathrm{L}\beta 1}) - E(\mathrm{Ge}_{\mathrm{L}\alpha 1}) = 30 \text{ eV} \tag{3.2}$$

We confirm this suspicion by looking into Figure 7 at the peak located at $E_{\mathrm{Ge}} = 1.205$ whilst not being able to determine the distinction between the two transition peaks.

3.2. Spectra for 15 kV acceleration voltage

No we will go over the spectra that we obtained as we increased the beam energy with an acceleration voltage of 15 kV. As in Figure 7 we will remove the strobe peaks to increase visibility.

In Figure 8 we see the distinct peaks that correspond to the Kα_1 and Kβ_1 transitions of Silicon in each spectrum for the substrate and the island. These have been counted in really high amounts compared to the energies corresponding to

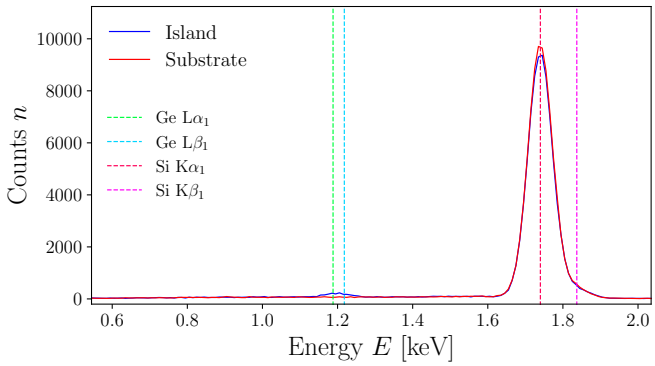

Figure 8: X-ray energies E counted by the XFlash detector on the position of an island and on the substrate itself with acceleration voltage 15 kV.

the energies for the L transitions of Germanium. We will look at the plot from Figure 8 with a logarithmic scale. The logarithmic scale allows us to the see that the resolution at 15 kV is still not good enough to distinct the peaks for Ge nor Si. But here we have a better view on the contribution

of the Kβ_1 transition energies that bulge out the spectrum for both the substrate and the islands for energies bigger than 1.7 eV.

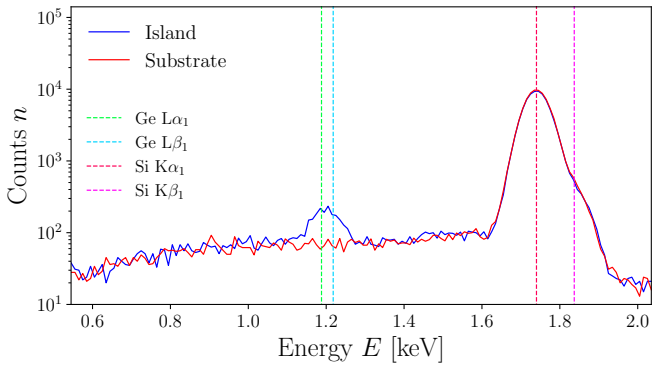

Figure 9: X-ray energies E counted by the XFlash detector on the position of an island and on the substrate itself with acceleration voltage 15 kV in log scale.

3.3. Comparison with respect to beam energy

Comparing the resulting spectra at 5 kV and 15 kV in Figure 7 and Figure 8 again give us information of how important the penetration depth of the interaction volume is.

The X-rays that result from the scattering events inside the sample are getting measured by the EDS detector. If we increase the beam energy from 5 kV to 15 kV the dimension of the penetration depth of the interaction volume increases. This will lead to the collection of X-rays that originate from deep within the sample. So deep in fact that the fraction of X-rays originating from the Si substrate is bigger than the one of X-rays originating from the (Si,Ge) islands. This is illustrated in Figure 10 where an interaction volume for an incident beam of 20 keV is simulated.

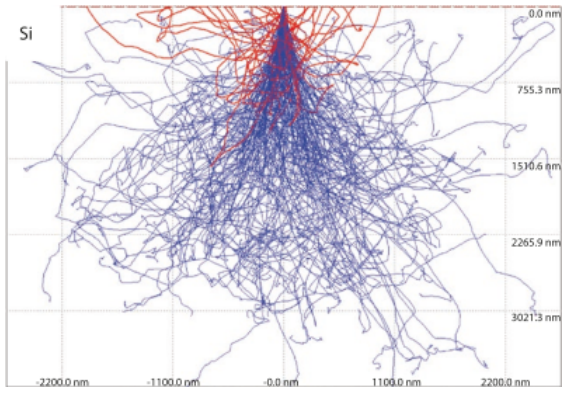

Figure 10: Simulated interaction volume for a beam energy of 20 keV. Taken from [Gol+18] Figure 1.8.

The penetration depth is in the dimensions of µm so it will not surprise us that for 15 kV acceleration voltage the counts for Si transition energies in Figure 8 is much higher than the counts for Ge transition energies.

To determine the ratio of Ge to Si in the island we simply compared the amount of counts in the peaks of Figure 7 because here we have the minimal penetration depth that would the determination of the chemical composition of the (Si,Ge) islands. With this technique we obtained a ratio of

$$\frac{\text{Si}}{\text{Ge}} = 0.28 \tag{3.3}$$

It is noteworthy that for higher beam energies we observed higher energie transitions for Ge noted in Table 3.

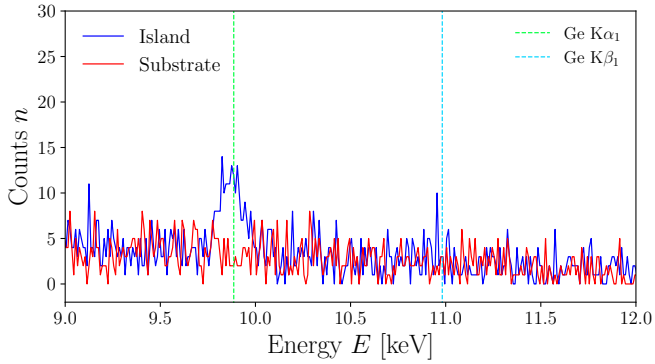

Figure 11: X-ray energies observed for 15 kV acceleration voltage. Higher characteristic X-ray transitions of Ge displayed.

Figure 11 shows that through the higher beam energy it is possible to see transitions that are much less probable. The Kα_1 and Kβ_1 for Ge were not visible in the spectrum when using 5 kV acceleration voltage.

3.4. Elemental maps

With our EDS detector we were able to spatially resolve the chemical composition of the sample.

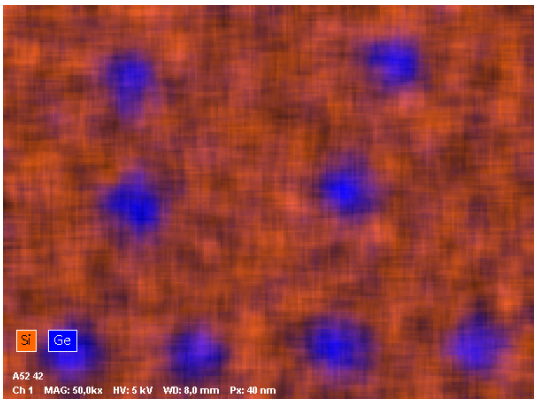

Figure 12: Spatially resolved chemical composition of the sample at 5 kV acceleration voltage.

Here the argument of the size of the interaction volume mentioned in Section 3.3 is shown in the lateral way. Increasing the beam energy increases the lateral size of the interaction volume. This will cause the spatial mapping to be faulty because the information gathered from X-rays

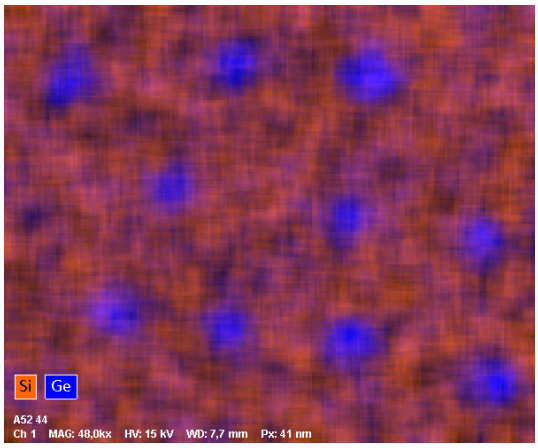

Figure 13: Spatially resolved chemical composition of the sample at 15 kV acceleration voltage.

that originated in the (Si,Ge) island could be mapped to a pixel that is not in the position of an island. This is clearly visible in Figure 13 as the blue color tints the space beyond the extend of the islands.

4. Discussion

4.1. Image quality are subject to skill

As we progressed in our endeavor to obtain high quality gray scale images we got better at controlling the SEM. The pictures shown in Section 1 are the result of a learning curve which shows in the first images for the acceleration voltage of 15 kV with the inlens detector where we struggled with the focus. Nonetheless as we carried out the instructions and advises from our instructor we were able to obtain images of sufficient quality.

4.2. Height Determination

The standard deviation of the height turned out to be surprisingly small, as it is not significantly bigger than the lowest possible uncertainty, given by the pixel size. The true systematic uncertainty is probably bigger than the one we used, as big contributions to the uncertainty stem from a low resolution and contrast in the image, as well as noise. This made it difficult to discern the edges of the top facet as well as of the islands themselves. This hidden uncertainty could have been cut down by using a larger zoom factor and increasing the exposure time.

We could also have used better methods to detect both the edges of the islands and their top facets, by further studying the behavior of images obtained using the SEM around both concave and convex edges and numerically searching for them. For example by numerically finding local minima or maxima and cutting the images there. However, for such an approach a higher resolution and contrast becomes even more important, as it would be difficult to rectify noise and slight deviations from the expected form of the data compared to doing it manually. On the other hand it would make the process of finding the top facet more quantifiable. With the method of only using one's own perception it is hard to say where exactly deviations in the determination came from, whereas when doing it numerically they could have been analyzed and maybe even rectified by refining the algorithm used.

With all these factors combined it is no surprise that the height of the frustums calculated in [Zhe+12] of 60 nm lies outside the range of the one we calculated.

4.3. Improving the resolution of the spectra

As mentioned in [WW03] the strobe peak in Section 3 can be used to improve the resolution of EDS. Because the strobe peak can be seen as the spread function of the detector via deconvolution it is possible to improve the spectrum resolution. Applying such an algorithm in our case could help to distinguish the L and K transitions energy peaks of Silicon and Germanium.

4.4. Drift in acquisition of spectra

As we recorded the spectra, the specimen was subject to significant drift. We recorded images at 15 kV acceleration voltage to illustrate this.

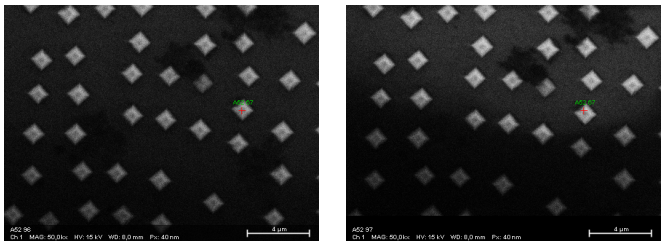

Figure 14: Illustration of the significant drift the specimen is undergoing at 15 keV beam energy.

This drift in Figure 14 can cause the spectrum to be faulty if the drifting distance is bigger than half of the characteristic base length of a frustum. But because of the size of interaction volume at 15 kV the spectrum will inevitably be afflicted with error.

5. Conclusion

While preparing and conducting the experiment we learned a lot about the modern ways of electron microscopes and their detectors. We learned that the Inlens detector is a phenomenal tool for imaging nanostructures like the frustums we encountered in this experiment. With the captured images from the detector we were able to extract the mean height of the frustums to be 51(8) nm. This value with its corresponding uncertainty lies outside of the range of the given value of 60 nm in [Par+16] where we suggested to use a numeric algorithm that will manage the acquisition of the data necessary for the determination of the height.

In conclusion the GeminiSEM 500 represent state of the art technology to analyze specimen regrading their topological relief, their chemical composition and spatially resolved composition.

References

[Bru] Bruker Corporation. *Periodic Table of Elements and X-ray Energies*. URL: https://usermanual.wiki/Pdf/PeriodicTableandXrayEnergies.1969160263/view.

[Car] Carl Zeiss Microscopy GmbH. *ZEISS GeminiSEM-Familie Produktinformation*. URL: https://www.tu-ilmenau.de/fileadmin/Bereiche/EI/mne-nano/Dokumente_Geraete/DE_40_011_095_GeminiSEM_rel_2_0_1_.pdf.

[Gol+18] J. I. Goldstein, D. E. Newbury, J. R. Micheal, N. W. M. Ritchie, J. H. J. Scott, and D. C. Joy. *Scanning Electron Microscopy and X-Ray Microanalysis*. Fourth Edition. Springer Nature, 2018, pp. 198–200. ISBN: 978-1-4939-6674-5.

[Mar+99] M. C. Martins, M. I. Marques, F. Parente, and J. G. Ferreira. "Some K x-ray relative transition probabilities for $Z = 47, 49, 52, 55$ and 56". In: *Journal of Physics B Atomic Molecular and Optical Physics* (1999).

[Par+16] A. Parvizi, W. Van den Broek, H. Kirmse, and C. T. Koch. *Spatially-Resvoled Elemental Analysis In The Scanning Electron Microscope*. AG Strukturforschung/Elektronenmikroskopie, Humboldt Universität zu Berlin, 2016. URL: https://www.physik.hu-berlin.de/en/sem/.

[SE72] V. W. Slivinsky and P. J. Ebert. "Kβ/Kα X-Ray Transition-Probability Ratios for Elements $18 \leq Z \leq 39$". In: *Physical Review A*. Third Series Volume 5 (No. 4 1972). DOI: https://doi.org/10.1103/PhysRevA.5.1581.

[WW03] M. Watanabe and D. B. Williams. "Improvements to Energy Resolution of an X-ray Energy Dispersive Spectrum by Deconvolution Using the Zero Strobe Peak". In: *Microscopy and Microanalysis* (2003).

[Zhe+12] C. L. Zheng, K. Scheerschmidt, H. Kirmse, I. Häusler, and W. Neumann. "Imaging of three-dimensional (Si,Ge) nanostructures by off-axis electron holography". In: *Ultramicroscopy* (2012).